Tellus (2007), 59A, 683–694
Printed in Singapore. All rights reserved

TELLUS

Hydrological cycle and ocean stratification in a coupled climate system: a theoretical study

By HSIEN-WANG OU*, *Lamont-Doherty Earth Observatory, Columbia University, Palisades, New York*

(Manuscript received 3 January 2007; in final form 10 May 2007)

ABSTRACT

As a logical progression of a deductive climate theory, this paper addresses three interconnected climatic features: the humidity profile, the atmospheric water transport and the ocean stratification—taking as given the thermal field previously determined. The theory invokes the maximization of the entropy production, which propels the tropospheric temperature and specific humidity to their updraft values, yielding moist-adiabatic lapse rate and bi-modal relative humidity in the vertical. With the humidity profile known, the atmospheric water transport at mid-latitudes can be linked to the thermal field, which then determines the ocean salinity range. The deduced density ratio across the thermocline however is quite larger than unity, suggesting considerable static stability.

The model deductions, while crude, are consistent with observations, which underscore the internal control of the hydrological cycle and ocean stratification by energy balances, with significant implications on climate changes. Doubling the atmospheric CO_2, for example, only slightly perturbs the energy balance and with it the global precipitation and the high relative humidity near the surface. The warming would however more strongly enhance the atmospheric water transport to accentuate the zonal-mean E-P pattern and ocean salinity contrast.

1. Introduction

This paper represents a continuing effort of the author to construct a deductive theory of the earth's climate given only the solar insolation (Ou, 2001, 2006, referred hereafter as Ou01 and Ou06, respectively). As a closure assumption, the theory invokes the maximized entropy production (MEP)—a selection rule for non-equilibrium turbulent systems and readers are referred to Ozawa et al. (2003) and Kleidon and Lorenz (2005) for comprehensive reviews of the MEP. As also discussed in Ou06, recent developments have significantly strengthened the physical basis of the MEP and alleviated some early criticisms. For example, since the macroscopic indeterminacy is rooted in turbulence, it is the material (not radiative) entropy production that is maximized; and with the turbulence being internal to the fluid, the MEP should apply to both climatic fluids individually.

Although such selection rule is not particularly amendable to GCMs' forward integration, recent calculations nonetheless showed that both ocean and atmosphere would assume higher entropy-production state when allowed (Shimokawa and Ozawa, 2002; Kleidon et al., 2003), in consistency with the MEP. In short, based on recent advances along multiple fronts—theoretical, experimental and computational, the MEP has emerged as a viable counterpart to the second fundamental law for non-linear non-equilibrium thermodynamic system; we are thus justified to posit it as a working hypothesis in the construction of our theory.

Through global-mean balances, Ou01 first determined, among other things, the surface temperature and found it to be narrowly constrained by intrinsic properties of water and since the required energy balances can be maintained over a wide range of the solar constant, the derivation may resolve the 'faint young sun' paradox. With the global-mean fields known, Ou06 then derived the meridional thermal field, and found that both ocean and atmosphere are divided into warm and cold masses by mid-latitude fronts, consistent with the first-order description of the observed state. The derivation reinforces the pre-eminent role played by the water triple-point in anchoring and stabilizing the thermal field (Webster, 1994).

As a logical progression of the theory, this paper addresses three important and closely related climate features: the humidity profile, the atmospheric water transport, and the ocean stratification. The humidity profile affects radiative fluxes and hence the energy balance considered by Ou01, which however did not deduce this profile, but used instead the calculated LW fluxes—an acknowledged gap in the model closure. It is seen here that the MEP provides a simple rationale for constraining the moisture field, thus may remedy this shortfall. With the moisture profile known, we then proceed to derive the atmospheric water transport at mid-latitudes, which is linked simply to the thermal field and hence known as well. When combined with the thermal

*Correspondence.
e-mail: dou@ldeo.columbia.edu
DOI: 10.1111/j.1600-0870.2007.00259.x

contrast of the ocean, this water transport then specifies the ocean stratification, an important property in the general ocean circulation.

Besides providing internal linkages of the theory, these features are among the defining characteristics of the earth's climate, whose explanations are thus important in our understanding of the climate. In addition, the roles of the hydrological cycle and ocean stratification are particularly accentuated in recent studies of climate changes (Bryan, 1986; Manabe and Stouffer, 1994; Held and Soden, 2000); and although our theory is concerned with the climatic steady-state, by underscoring the internal control of these properties, it nonetheless has important implications on climate changes. The three subjects are discussed in sequential order in Sections 2–4. The main findings are summarized in Section 5 as well as discussion of their broader implications.

2. Humidity profile

Water vapour is the dominant greenhouse gas and strong SW absorber in the earth's atmosphere; its height distribution thus directly affects the energy balance of the earth's system. While there is much discussion of the moistening processes in the atmosphere, we remain uncertain about the balance requirements that control the humidity profile. To address this question, we consider a model configuration similar to that of Ou01 (Fig. 1) in which the troposphere is divided into a planetary boundary layer (PBL) capped by the lifting condensation level (LCL) and a free troposphere above the LCL characterized by deep updrafts embedded in vast ambience of slow subsidence. Since the actual troposphere cannot be easily cast in this simple form, the model should be regarded as conceptual, which nonetheless suffices in elucidating some essential climate features.

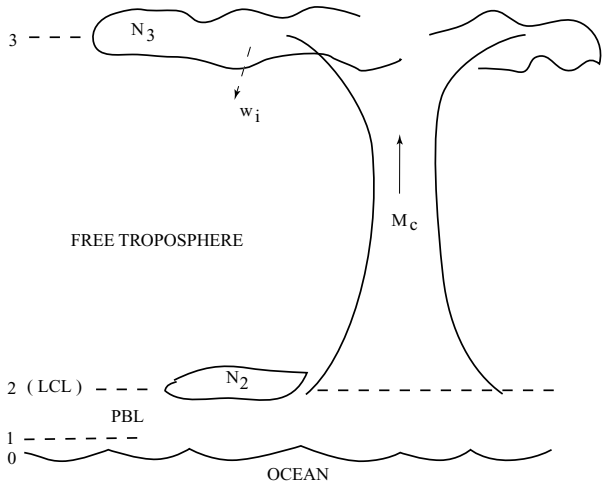

Fig. 1. A conceptual scheme for the troposphere, which is divided into a planetary boundary layer (PBL) capped by the lifting condensation level (LCL) and a free troposphere above the LCL composed of deep updrafts embedded in vast ambience. Air is saturated and moist-adiabatic in the deep updraft, and the ambient temperature and humidity are subjected to the MEP and global balances.

Since the latent heat is not released below the LCL, the turbulence in the PBL is fuelled by the sensible heat from the surface, which however is largely expended by the radiative cooling in the PBL and from the shallow cloud top—as the latter marks the termination of such turbulence. The deep updrafts on the other hand are driven mainly by latent heat released by condensation, whose capping at the tropopause causes out-flowing air and expansive high clouds. It is for this reason that Ou01 linked the cumulus mass flux to the high-cloud cover constrained by the energy balance, a key step in the later closure of the moist convection.

In terms of the moisture budget, the deep updraft constitutes the only conduit for the upward transport of water out of the PBL, which moistens the ambient air through detrainment, horizontal mixing or evaporation of hydrometeors (Sun and Lindzen, 1993; Sui et al., 1994; Pierrehumbert, 1998)—although, as we shall see, one need not be specific about these processes in determining the climatic state governed by balance requirements. While the deep updraft would entrain the ambient air, we assume the mixing timescale to be long compared with the air transit time through the updraft (Sun and Lindzen, 1993) that its core remains saturated and hence characterized by moist-adiabatic lapse rate. As such, the temperature and moisture profiles in the updraft are known from Ou01, to which the ambient profiles are to be referenced. The latter, on the other hand, are what determine the radiative cooling of the troposphere given the small areal coverage of the deep updraft, and since this radiative cooling must be balanced by convective heating—the irreversible source of entropy in the present application (see Section 1), one perceives the possibility that the MEP may propel the ambient fields, as seen next.

2.1. Maximized LW opacity

As a first step in our derivation, we shall see that the MEP would maximize the LW opacity of the troposphere, so the ambient specific humidity is propelled towards the (saturated) updraft value. We adopt the terminology of Ou01 so the surface, the anemometer height, the LCL and the tropopause are designated levels 0, 1, 2 and 3, respectively. Since entropy of the troposphere is constant in the steady-state, we have

$$\frac{\mathrm{d}S}{\mathrm{d}t} = \int_0^3 \frac{1}{T}\mathrm{d}F_\mathrm{r} + \int_0^3 \frac{1}{T}\mathrm{d}F_\mathrm{c} = 0, \tag{1}$$

where the variables are global horizontal means, and F_r and F_c are 'radiative (LW)' and 'convective' fluxes respectively, taken to be positive upward. For simplicity, we have neglected the SW absorption since it is dominated by the LW cooling and hence does not affect the moisture tendency deduced below. The energy

balance states on the other hand

$$\int_0^3 \mathrm{d}F_\mathrm{r} + \int_0^3 \mathrm{d}F_\mathrm{c} = 0, \tag{2}$$

leading to

$$F_{\mathrm{r},3} - F_{\mathrm{r},0} = F_{\mathrm{c},0}, \tag{3}$$

or the net radiative cooling of the troposphere (the left-hand side, LHS) equals the convective flux entering its lower boundary (the right-hand side, RHS). Defining a radiative cooling temperature T_r by (see Emanuel and Bister, 1996)

$$\frac{1}{T_\mathrm{r}} \int_0^3 \mathrm{d}F_\mathrm{r} \equiv \int_0^3 \frac{1}{T} \mathrm{d}F_\mathrm{r}, \tag{4}$$

$$= \frac{C_p}{g} \int_0^3 \frac{1}{T} \dot{T} \mathrm{d}p, \tag{5}$$

where C_p is the specific heat at constant pressure, g, the gravitational acceleration and $\dot{T}$, the radiative cooling rate, then the irreversible entropy production, when subjected to eqs (1), (3) and (4), yields (see also Pauluis and Held, 2002)

$$\left(\frac{\mathrm{d}S}{\mathrm{d}t}\right)_\mathrm{irr} = \int_0^3 F_\mathrm{c} \mathrm{d}\left(\frac{1}{T}\right), \tag{6}$$

$$= F_{\mathrm{c},0} \left(\frac{1}{T_\mathrm{r}} - \frac{1}{T_0}\right). \tag{7}$$

This equation states simply that the entropy produced in the troposphere by irreversible processes (eq. 6) must exit through its boundaries (eq. 7), the latter a consequence of (convective) heating and (radiative) cooling at different temperature. It should be noted that since we are concerned with entropy production in the troposphere, the air–sea temperature difference plays no part in our consideration.

The second law states that eq. (7) is positive, or the radiative cooling temperature be lower than the surface temperature where the convective flux enters the troposphere; the MEP states in addition that eq. (7) be maximized, which thus maximizes the surface convective flux and minimizes the radiative cooling temperature—to the degree that they are affected by the moisture content in the present discussion. It should be noted that this radiative cooling temperature is *not* the emission temperature of the OLR, but rather the mean temperature (when inverted) weighted by the cooling rate, which need not be strongly affected by the humidity level. In fact, should the cooling rate $\dot{T}$ be vertically uniform,[1] and neglecting the tropopause pressure, it is seen that $T_\mathrm{r} \approx T_0(1 - \gamma R_\mathrm{d}/g)$, where γ is the lapse rate, taken to be constant, and R_d is the gas constant of the dry air. A lapse rate of $\gamma \approx 6.5\ \mathrm{K\,km^{-1}}$, for example, would yield $T_\mathrm{r} \approx 0.81 T_0$ and a thermodynamic efficiency of about 20% if the atmosphere operates as a Carnot engine.

With the above discussion, we see that the temperature contrast in eq. (7) is not directly affected by the moisture level; to maximize eq. (7), it suffices therefore to seek the moisture field that maximizes the surface convective flux $F_{\mathrm{c},0}$—same as the net radiative cooling (eq. 3). Now the key step is in recognizing that the latter increases with the LW opacity (see, for example Lorenz and McKay, 2003), so the moisture content is maximized. As a possible computational support of this deduction, we invoke numerical calculations of Renno (1997), which have included explicit hydrological cycle, so the moisture field may freely evolve. He found that with the present solar forcing, multiple states of differing moisture content are allowed and the higher humidity state (of greater entropy production) is the one that is likely realized.

Given the temperature dependence of the saturation vapour pressure via the Clausius–Clapeyron equation (referred as CC scaling below), the above maximization of the moisture content implies that both ambient temperature and specific humidity should approach their updraft values. As we shall see later, there are limitations as to how close these approaches could be, but, given this tendency, one is justified to assume a priori that the departures from the (known) updraft profiles to be sufficiently small that the radiative cooling can be calculated. This approximation is aided by the realization that, because of the strong LW absorption by the water vapour, the radiative cooling would have levelled off (or the greenhouse effect is 'saturated') even with a moderate degree of saturation (Hartmann and Michelsen, 1993; Pierrehumbert, 1995). With the specification of the radiative and hence convective fluxes, one may then apply entropy and energy balances to determine the actual departure of the ambient temperature and humidity from their updraft profiles. If they indeed are comparable to that observed, then the above approximation of saturated greenhouse effect is validated and need not constitute a limitation of the theory. With the specification of the radiative fluxes, we have also bridged a significant gap in the closure of Ou01, an important objective of the study as alluded to in the introduction.

2.2. *Dominant latent heat flux*

In the above, we have seen that the MEP, through its maximization of the LW opacity, allows a priori assumption of saturated greenhouse effect, so the radiative and—hence—convective fluxes are in principle known. Since the convective flux consists of both sensible and latent heat, it cannot yet be used to constrain the ambient humidity. To this aim, we shall see next that the convective flux in the free troposphere is in fact dominated by the latent heat due to the low efficiency of the atmospheric heat engine.

We begin by noting that the irreversible entropy production can be linked to the mechanical work via (e.g. Pauluis and Held,

[1]This feature need not be related to the moisture level, and is indeed a good approximation of the present climate in the clear sky (see fig. 8b of Manabe and Strickler, 1964).

2002)

$$\eta F_{c,2} \approx M_c \int_2^3 g\left(\frac{T'}{\bar{T}} + 0.608q'\right)\mathrm{d}z, \tag{8}$$

where η is the thermodynamic efficiency, M_c, the mass flux of the undiluted core, q, the specific humidity, and overbars and primes denote, respectively, the global horizontal means and the ambient deficits from the updraft values. The integral on the RHS represents the Convective Available Potential Energy (CAPE) of the free troposphere, and with the convective and mass fluxes now known (the latter from Ou01), so is the CAPE if one knows the efficiency of the atmospheric heat engine. This efficiency is bounded above by that of the Carnot engine estimated earlier to be about 0.2, but is otherwise highly uncertain given the myriad moisture processes that are irreversible and yet produce no mechanical work (Pauluis and Held, 2002). It is reasonable however to assume that $\eta \leq$ O (0.1) based on observations (for example, Lorenz, 1967), which suffices for the following scale derivation. From eq. (8), we see that, since $q\prime$ is positive (the ambient air may not be super-saturated),

$$\frac{[T']}{\bar{T}} \leq \frac{\eta}{gH}\frac{F_{c,2}}{M_c}, \tag{9}$$

where the bracket indicates a scale, and H is the tropopause height. For an order-of-magnitude estimate, one may use $H =$ 15 km, $F_{c,2} = 60\ \mathrm{W\,m^{-2}}$ and $M_c = 10^{-2}\mathrm{kg\ m^{-2}\,s^{-1}}$ (all these are known from previous derivations, including Ou01, see also footnote[2]), which yields a temperature deficit of no more than a few degrees, or the temperature in the ambient air is in effect equilibrated to that in the deep updraft. Physically, there is simply not enough conversion of internal to mechanical energy to sustain a greater CAPE, which thus may explain why the tropospheric lapse rate is moist-adiabatic—as in the deep updraft even though the latter occupies only a tiny fraction of the global area (less than one percent). Incidentally, this deduction of the CAPE as merely an equilibrium response to the moist convection, rather than its driver, reinforces the view advanced by Emanuel et al. (1994), which has downplayed the dynamical significance of CAPE or its usefulness as a gauge of the strength of the moist convection.

With the ambient temperature equilibrated to the updraft temperature, one expects the sensible heat flux to be small. A more general derivation however is possible by noting from eq. (9) that

$$M_c C_p [T'] \leq \left(\frac{C_p \bar{T}}{gH}\right)\eta F_{c,2} \tag{10}$$

$$\ll F_c \tag{11}$$

since the value in the parenthesis is of O (1) for the tropospheric temperature range. As a consequence,

$$F_c = M_c(C_p T' + Lq') \tag{12}$$

$$\approx M_c L q', \tag{13}$$

or the convective flux carries mainly the latent heat, a deduction consistent with model calculations that have resolved moist convection (Sui et al., 1994; Pauluis and Held, 2002). Note that the above derivation has made no reference to the magnitude of the convective or mass flux, it is thus more general than that entailed in eq. (9), and since eq. (11) is due primarily to the low efficiency of the atmospheric heat engine (that is, $\eta \ll 1$), the latter thus may be attributed the cause for the dominance of the latent heat flux. This deduction reinforces the earlier argument (see also Ou01) that the sensible heat flux from the surface is largely depleted before it reaches the free troposphere. From the energy balance (eq. 13), one sees, in addition, that although the ambient humidity is propelled towards saturation by the MEP (that is, $q' \to 0$), this approach is curtailed by the finiteness of the convective and mass flux. In other words, if the ambient air were to saturate, then the convective heat flux, being dominated by the latent heat, would vanish and cannot balance the radiative cooling.

2.3. Ambient vapour pressure

With the approximation (eq. 13), one may then proceed to calculate the deficit of the ambient specific humidity q' given the convective heat flux F_c and cumulus mass flux M_c (known from Section 2.1 and Ou01). For observational comparisons, the ambient humidity profile can be expressed in terms of the vapour pressure as a function of the temperature, as shown schematically in Fig. 2 (the dashed line). This is to be contrasted with the saturation curve (the thin solid line) that characterizes the deep updraft. Although the present derivation applies only to the free troposphere above the LCL, one may assume linear mixing of specific humidity and potential temperature (conserved for dry convection) in the PBL, as indicated by the dotted line in the figure. Together with the dashed line, we have then a full-depth description of the ambient humidity.

For a crude assessment of the ambient humidity in the free troposphere, the following scale derivation seems sufficient. We begin with the energy balance

$$F_c = -\frac{C_p}{g}\int_{p_3}^{p} \dot{T}\,\mathrm{d}p, \tag{14}$$

which states that the convective flux at any level equals the net radiative cooling above that level. Assuming a uniform cooling rate (see footnote 1) and neglecting the tropopause pressure (the following derivation thus does not apply to the upper troposphere), eq. (14) implies a convective flux linear in pressure,

[2]Correcting an error in Ou01, it is the mass not the volume flux that is conserved, which is then linked to the high-cloud cover N_3 via $M_c \approx \rho_3 w_i N_3$, with w_i being the ice settling velocity. Setting $\rho_3 = 0.4\,\mathrm{kg\ m^{-3}}$, $w_i = 0.05\ \mathrm{m\ s^{-1}}$ and $N_3 = 0.5$ (see Ou01), we estimate a mass flux of $10^{-2}\ \mathrm{kg\ m^{-2}\ s^{-1}}$, which is consistent with fig. 15.7 of Emanuel (1994).

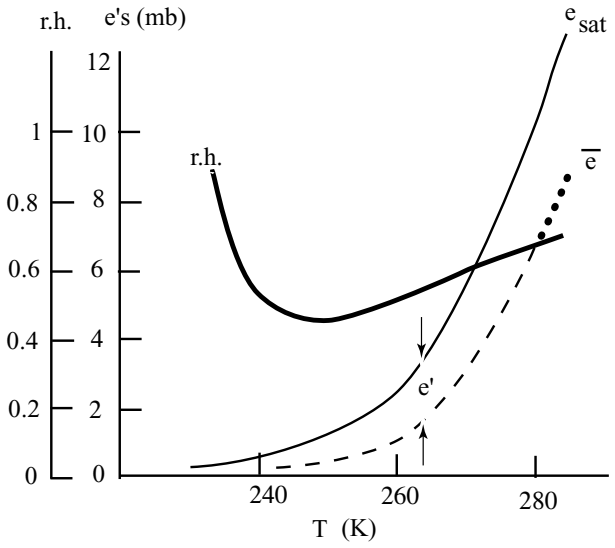

Fig. 2. The water-vapour pressure plotted against temperature. The thin solid and dashed lines are for the updraft (saturated) and its ambience, respectively, and the dotted line, the extension of the ambient curve into the PBL. The ambient curve trends as the saturation curve since the radiative cooling does not vary strongly in height, and the curve is based on actual model calculation. The thick solid line is the corresponding relative humidity, which shows a mid-tropospheric minimum.

or

$$\mathrm{d}\ln F_{\mathrm{c}} \sim \mathrm{d}\ln p, \tag{15}$$

with the symbol '$\sim$' signifying a scale relation. With eq. (13) and $q' \approx 0.622e'/p$, we have then

$$\mathrm{d}\ln e' \sim 2\mathrm{d}\ln p \tag{16}$$

$$\sim \frac{2g}{R_{\mathrm{d}}\gamma}\mathrm{d}\ln T, \tag{17}$$

which gives a power dependence of the vapour–pressure deficit on the temperature. The saturation curve on the other hand is given by the Clausius–Clapeyron equation

$$\mathrm{d}\ln e_{\mathrm{sat}} = \frac{T_{\mathrm{c}}}{T}\mathrm{d}\ln T, \tag{18}$$

where $T_{\mathrm{c}} \equiv 0.622L/R_{\mathrm{d}} \approx 5420\,\mathrm{K}$, so the ratio of the two yields

$$\frac{\mathrm{d}\ln e'}{\mathrm{d}\ln e_{\mathrm{sat}}} \sim \frac{2gT}{R_{\mathrm{d}}\gamma T_{\mathrm{c}}}, \tag{19}$$

which gives a crude measure of the variation of the spacing between the two curves in Fig. 2 relative to that of the saturation curve. If one uses a LCL temperature of 280 K and a lapse rate of 6.5 K km^{-1}, this ratio is 0.55, quite smaller than unity (even smaller for lower temperature), which implies a similar trending of the ambient vapour–pressure as the saturation curve. This is a pronounced feature in observations (Webster, 1994), which thus can be explained. The deduction is also consistent with the observation that the sea surface temperature constitutes the main determinant of the precipitable water in the overlying column, buffering the effect of the atmospheric circulation (Stephens, 1990).

This similar trending aside, the ambient curve still merges with the saturation curve in the upper troposphere where the convective flux vanishes. As such, the relative humidity (the thick solid line) should be bi-modal in the vertical with a minimum in the middle troposphere, a feature indeed discernible in observations (Folkins et al., 2002) and numerical calculations that have resolved the moist convection (Held et al., 1993; Robe and Emanuel, 1996). The ambient curve and the relative humidity shown in Fig. 2 correspond incidentally to the actual calculation from eq. (13) assuming uniform cooling rate [hence a convective flux linear in the pressure (eq. 14)] and the specifications that $F_{\mathrm{c},2} = 60\,\mathrm{W\,m^{-2}}$, $M_{\mathrm{c}} = 10^{-2}\,\mathrm{kg\,m^{-2}\,s^{-1}}$, $\gamma = 6.5\,\mathrm{K\,km^{-1}}$, $p_2 = 850$ mb, $p_3 = 300$ mb and $T_2 = 280$ K (all assumed known from Ou01). The resemblance of the calculated to the observed curves (Webster, 1994, his fig. 3) lends support to eq. (13) or that the ambient humidity is constrained by global energy balance.

With this proposition, some inferences can be drawn. For example, although the specific humidity in the ambient air parcel is largely conserved (Pierrehumbert and Roca, 1998), such consideration does not constrain the humidity profile since the air motion—including where it detrains from the deep updraft—is an internal property. Nor should the ambient humidity profile be affected by microphysics (Dessler and Sherwood, 2000), which has only minor effect on the energy balance. And with the humidity internally constrained, there is little justification for fixing the relative humidity profile in climate-change studies (Manabe

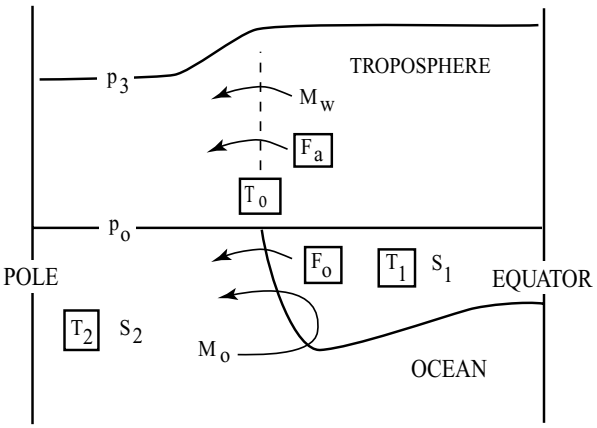

Fig. 3. The model configuration for the derivation of the atmospheric water transport and ocean stratification. The ocean is divided into warm and cold water-masses, and the thermal properties enclosed in boxes are assumed known from Ou06, which include the surface air temperature (T_0), the atmospheric heat transport (F_{a}), the temperature of the two water-masses (T_1 and T_2), and the oceanic heat transport across the front (F_{o}).

and Wetherald, 1967) or for independently varying the humidity to examine its effect on the OLR (Spencer and Braswell, 1997) or the surface temperature (Shine and Sinha, 1991). Moreover, to the degree that the convective mass flux is known from global balances (see Ou01), so is the compensating subsidence, which may not balance the radiative cooling (the shortfall can be bridged by horizontal mixing) and one may not use such balance to constrain the convective mass flux (Knutson and Manabe, 1995).

3. Atmospheric water transport

Having deduced the humidity profile, we may now seek to link the vapour transport at mid-latitudes to the thermal field known from Ou06, which are enclosed in boxes in Fig. 3. The derivation is limited to mid-latitudes for the reasons that: (1) at these latitudes, vapour transport is dominated by eddies, the same process that transports the energy, thus allowing their linkage; (2) the warm and cold water-masses are separated at the surface at mid-latitudes (the subtropical front), so it is the vapour transport across mid-latitudes that differentiate their salinity and (3) at low latitudes, much of the vapour transport is facilitated by the meridional wind in the PBL, which is linked by the Ekman dynamics to the zonal wind not yet known from the theory.

3.1. Meridional Bowen ratio

Since the atmospheric water transport is mainly in the vapour form (Peixoto and Oort, 1992, hereafter PO92), it is proportional to the latent-heat transport; one thus needs to first deduce how the atmospheric heat transport may be partitioned between the sensible and latent components. With F_s and F_l denoting the zonal-mean sensible- and latent-heat transports, respectively, we define a 'meridional' Bowen ratio

$$Bo_{\mathrm{m}} \equiv F_{\mathrm{s}}/F_{\mathrm{l}}, \tag{20}$$

which will be referred simply as Bowen ratio for convenience. Let overbars and primes denote the zonal means and eddy-induced deviations respectively, and neglecting the complication associated with the PBL given its shallowness, we derive

$$\begin{aligned} F_{\mathrm{l}} &= L\int_{p_3}^{p_0} \overline{v'q'}\,\mathrm{d}p \\ &= 0.622L\int_{p_3}^{p_0} \overline{v'e'}\frac{\mathrm{d}p}{p} \\ &\approx 0.622L\int_{p_3}^{p_0} \overline{v'T'}\frac{\mathrm{d}\bar{e}}{\mathrm{d}T}\frac{\mathrm{d}p}{p} \\ &\approx 0.622L\int_{p_3}^{p_0} \overline{v'T'}\frac{\mathrm{d}e_{\mathrm{sat}}}{\mathrm{d}T}\frac{\mathrm{d}p}{p} \end{aligned} \tag{21}$$

where v' represents the meridional wind associated with eddies. In the above, we have assumed that the vapour pressure is primarily a function of the temperature and that, as deduced above, the (zonal-mean) ambient vapour pressure trends as the saturation curve. Since synoptic eddies typically extend through the troposphere, the sensible heat flux $\overline{v'T'}$ is not a strong function of altitude—certainly much weaker than the term containing the vapour pressure, which thus can be replaced by its vertical average. Applying the same approximation to the other variables, eq. (21) can be written as

$$\begin{aligned} F_{\mathrm{l}} &\approx \frac{F_{\mathrm{s}}}{\Delta p}\frac{gT_{\mathrm{c}}}{\gamma C_p}\int_0^{e_{\mathrm{sat},0}}\frac{\mathrm{d}e_{\mathrm{sat}}}{T} \\ &\approx \frac{F_{\mathrm{s}}}{\Delta p}\frac{gT_{\mathrm{C}}}{\gamma C_p}\frac{e_{\mathrm{sat},0}}{T_0}, \end{aligned} \tag{22}$$

where $\Delta p \equiv p_0 - p_3$ is the pressure range of the troposphere. Substituting eq. (22) into eq. (20), we arrive at a simple formula for the Bowen ratio

$$Bo_{\mathrm{m}}^{-1} \approx \frac{T_C}{T_0}\frac{e_{\mathrm{sat},0}}{\Delta p}\frac{g}{\gamma C_p}. \tag{23}$$

It is noted that surface temperature enters this expression both explicitly and through the corresponding saturation vapour pressure. The two have opposite effects, but given the stronger variation of the latter, one expects the latent heat transport to increase in importance over the warmer surface. Besides the surface temperature, the only external parameters in eq. (23) are the tropopause pressure and the lapse rate; both however are relatively well constrained, suggesting that the expression may be credibly tested by observation. Setting $\Delta p = 700$ mb and

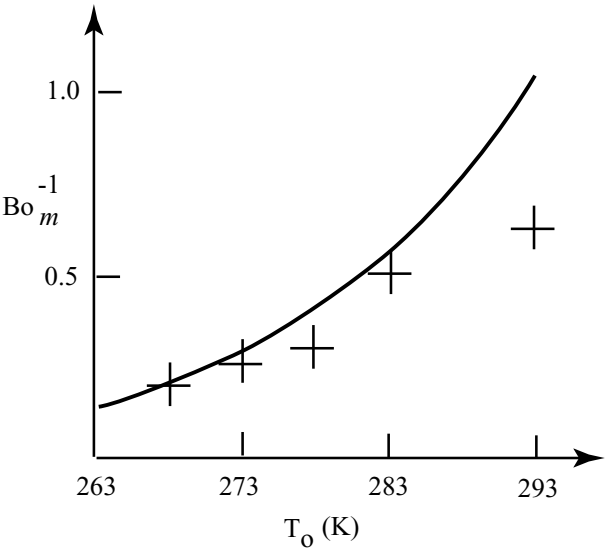

Fig. 4. The inverse of meridional Bowen ratio plotted as a function of the surface air temperature. The solid line is calculated from eq. (23) with Δp set to 700 mb, and crosses are observational estimates based on figs. 7.5, 12.12a and 13.6a of Peixoto and Oort (1992), taking values from 30, 40, 50, 60 and 70°N. The two are in close agreement in mid-latitudes where the model derivation is intended.

$\gamma = 6.5\ \mathrm{K\,km^{-1}}$, the value calculated from eq. (23) is plotted in Fig. 4 in the solid line, and we have plotted in crosses the observed values estimated from figs. 7.5, 12.12a and 13.6a of PO92 for selected latitudes. Considering the crudeness of the model derivation and uncertainty in the observed values, the agreement is surprisingly good, particularly over mid-latitudes where the model derivation is intended. It is interesting to note that because of its linear dependence on the saturation vapour pressure (eq. 23), the inverse Bowen ratio trends (approximately) the saturation curve shown in Fig. 2 over probable mid-latitude temperature range. But because of the water-vapour transport is concentrated in the lower troposphere while sensible-heat transport is not, this inverse Bowen ratio is typically less than one, much smaller than its surface counterpart.

3.2. Linkage to the thermal field

With the above validation of the partition of the sensible and latent heat transport, we may now proceed to link the atmospheric water transport to the energy transport. Since synoptic eddies, being quasi-geostrophic, transport little potential energy, and given the negligible transport of the kinetic energy (PO92, section 13.3.3.2), the atmospheric energy transport F_a at mid-latitudes consists mainly of sensible and latent heat

$$F_\mathrm{a} \approx F_\mathrm{s} + F_\mathrm{l}. \tag{24}$$

Let M_w be the atmospheric water transport, one has then

$$\begin{aligned} M_\mathrm{w} &\approx \int_{p_3}^{p_0} \overline{v'q'}\,\mathrm{d}p \\ &= \frac{1}{L} F_\mathrm{l} \\ &\approx \frac{F_\mathrm{a}}{L\left(1 + 1/Bo_\mathrm{m}^{-1}\right)}, \end{aligned} \tag{25}$$

using eqs (24) and (20). With the Bowen ratio given by eqs (23), (25) thus allows the calculation of the water transport given the surface temperature and the atmospheric energy transport, both known from energy balances (see Fig. 3).

As expected, the atmospheric water transport increases with both the heat transport and the surface temperature—the latter through a greater apportion of the heat transport to its latent form (Fig. 4). Because of this dual dependence, one expects the maximum water transport to occur equator-ward of the maximum heat transport, a deduction indeed consistent with observations (compare figs. 12.12a and 13.19b of PO92). A more quantitative comparison however is superfluous since it amounts to testing eq. (23) as the additional steps leading to eq. (25) are trivial.

4. Ocean stratification

Distinguishing the forced and free convective regimes, Ou06 has divided the ocean into warm and cold water-masses, consistent with a first-order description of the observed situation. Indeed, because of the prominence of the main thermocline and its surface manifestation—the subtropical front, two-layer approximation has been widely used in describing and understanding the general ocean circulation (e.g. Veronis, 1973). With the thermal field of such a two-layered ocean known from Ou06 (see Fig. 3) as well as the atmospheric water transport specified by eq. (25), we shall now examine the salinity contrast across the thermocline.

4.1. Salinity contrast

Observationally, the warm water-mass is saltier. This is a direct outcome of the poleward water transport in the atmosphere, which can only return in the ocean—thus enhancing the salinity of the warm water-mass. Qualitatively, the degree of enhancement should increase with the atmospheric water transport, but decrease with the vigour of the oceanic mass exchange as the latter acts to even out the salinity contrast. We have already seen that the atmospheric water transport is specified by the thermal field (eq. 25), and the oceanic mass exchange is precisely what transports the ocean heat and hence known, we hypothesize therefore that the salinity contrast is constrained by energy balance as well.

To formalize this hypothesis, let M_o denote the mass exchange rate between the warm and cold water-masses, then, since there is no heat source/sink in the deep water, it is linked to the oceanic heat transport across the frontal latitude F_o via

$$M_\mathrm{o} = (C_{p,\mathrm{o}} \Delta T_\mathrm{o})^{-1} F_\mathrm{o}, \tag{26}$$

where $C_{p,\mathrm{o}}$ is the specific heat of water at constant pressure and ΔT_o, the temperature difference of the two water masses. With the RHS known from Ou06 (see Fig. 3), so is the mass exchange rate, and one need not be specific about its partition between eddies migrating across the front and the Meridional Overturning Circulation (MOC). Nor should one be concerned with the variable mechanical energy input by wind since it could be accommodated by changing thermocline depth (see Section 4.3). Although a subtler point, it should also be mentioned that this mass exchange rate does not include the return (oceanic) branch of the hydrological cycle since the sensible heat carried by this return flow has physical meaning only when the warm water mass is lost through excessive E-P, which thus should be counted within the ocean heat transport F_o, and, in any event, small compared with the latent heat flux at the surface. Combining eqs (25) and (26) yields

$$\frac{M_\mathrm{w}}{M_\mathrm{o}} = \frac{C_{p,\mathrm{o}} \Delta T_\mathrm{o}}{L\left(1 + 1/Bo_\mathrm{m}^{-1}\right)} \frac{F_\mathrm{a}}{F_\mathrm{o}}. \tag{27}$$

Since the RHS is known from Ou06 (see Fig. 3) and eq. (23), so is this ratio, which is seen later to determine the salinity contrast across the thermocline. Since testing of such balances is not the objective here, to assess above expressions, one may simply use

the observe values for the thermal input. As a representative example, we set a frontal latitude at 40°N, so the surface air temperature is $T_0 = 283\ K$ (fig. 7.5 of PO92) with an inverse Bowen ratio of $Bo^{-1}{}_{\rm m} = 0.5$ (Fig. 4). Setting in addition $F_{\rm a} = 4$ PW, $F_{\rm o} = 1$ PW (based on Trenberth and Caron, 2001) and $\Delta T_{\rm o} = 20$ K (see fig. 8.8 of PO92), eq. (26) then yields $M_{\rm o} \approx 1.2 \times 10^{10}\ {\rm kg\,s^{-1}}$ (a volume transport of 12 *Sv*), and eq. (27) yields $M_{\rm w}/M_0 \approx 0.045$, giving rise to $M_{\rm w} \approx 5.4 \times 10^8\ {\rm kg\,s^{-1}}$ (or 0.54 *Sv*). The above value for the ocean mass transport is consistent with that calculated from GCMs (see, for example Wunsch, 2002, whose figure shows a transport of about 14 *Sv*); and the above atmospheric water transport is comparable to fig. 12.12 of PO92, which shows a value of 0.61 *Sv* at 40°N.

While the atmospheric water transport is negligible in the mass balance of the ocean, it is the *only* source that drives the ocean salinity contrast ΔS. Let the suffices '1' and '2' denote respectively the warm and cold water-masses (see Fig. 3), the salt balance of the warm water-mass is approximately (Stommel and Csanady, 1980)

$$M_{\rm w} S_2 = M_{\rm o} \Delta S, \tag{28}$$

which states that the salt influx carried by the return flow equals the salt outflux through the mass exchange. Rearranging, we have

$$\frac{\Delta S}{S_2} = \frac{M_{\rm w}}{M_{\rm o}}, \tag{29}$$

and given the smallness of the RHS as estimated above, so is the salinity enhancement relative to the cold water salinity; the latter thus can be replaced by the mean salinity $\bar{S}$, a property evolving on geological timescales and hence may be regarded as known. This equation merely reiterates the earlier statement that the salinity contrast is enhanced by the atmospheric water transport, but reduced by the water mass exchange. As a cursory check of its validity, we set $\bar{S} \approx 35$ (in psu) and use the above estimate of the RHS to yield a salinity range of 1.5, which is commensurate with that observed (see for example, fig. 8.12 of PO92, which gives a range of about 1.7). Combining eqs (27) and (29), we have

$$\frac{\Delta S}{\bar{S}} = \frac{C_{p,{\rm o}} \Delta T_{\rm o}}{L\left(1 + 1/Bo_{\rm m}^{-1}\right)} \frac{F_{\rm a}}{F_{\rm o}}, \tag{30}$$

or the salinity contrast is specified by the thermal field and hence controlled by energy balances, as we have set out to show.

4.2. Density ratio

Taking note of the linear dependence of the salinity range on the temperature contrast (eq. 30), one expects the density ratio to be independent of either and hence a more robust property, which moreover is what determines the static stability of the thermocline. Let α and β denote the thermal expansion and saline contraction coefficients, respectively, eq. (30) then yields the following expression for the density ratio

$$\begin{aligned} R_\rho &\equiv \frac{\alpha \Delta T_{\rm o}}{\beta \Delta S} \\ &\approx \frac{\alpha L}{\beta \bar{S} C_{p,{\rm o}}} \frac{F_{\rm o}}{F_{\rm a}} \left(1 + \frac{1}{Bo_{\rm m}^{-1}}\right) \\ &\approx 3.84 \times \frac{F_o}{F_a} \cdot \left(1 + \frac{1}{Bo_m^{-1}}\right). \end{aligned} \tag{31}$$

In eq. (31), we have inserted the values $\alpha = 1.7 \times 10^{-4}\ {\rm K^{-1}}$ and $\beta = 7.6 \times 10^{-4}$ (based on Neumann and Pierson, 1966, table V and VIII in appendix A), in addition to other parameter values cited earlier. As expected, the density ratio is independent of the thermal contrast in the ocean, but a function only of the heat transport partition and the Bowen ratio at the frontal latitude.

To assess the static stability of the thermocline, this density ratio is plotted in Fig. 5 over extensive ranges of these parameters. It is seen that increasing the atmospheric share of the heat transport (that is, moving leftward in the figure) or the surface air temperature (moving upward, see Fig. 4) enhances the effect of the atmospheric water transport in salinating the warm water, which reduces the density ratio. The solid dot corresponds to the thermal values cited earlier, which renders a density ratio of about 3 (or a buoyancy contrast of $2.3 \times 10^{-2}\ {\rm m\,s^{-2}}$). For observational validation, Stommel and Csanady (1980) found a density ratio of 2.8 in the North Atlantic (based on a slope of 12.5 in their fig. 1) and the most frequently observed value from

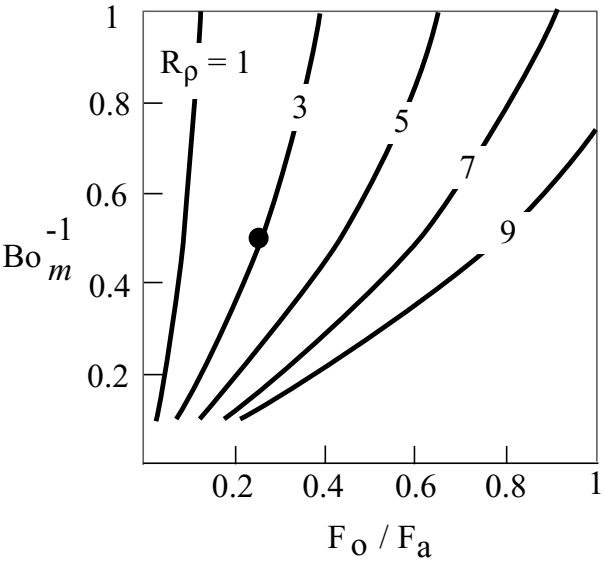

Fig. 5. The density ratio across the thermocline plotted against the heat transport ratio and the inverse Bowen ratio at the frontal latitude. The solid dot is the model value calculated from eq. (31), which is comparable to the observed value. Since this value is far above unity, the thermocline is unlikely to overturn.

census by Tippins and Tomczak (2003) is 3.2. Since these values are quite larger than unity, the thermocline should be rather stable; in fact, with the same surface air temperature at the frontal latitude, it requires more than doubling of the atmosphere/ocean heat transport ratio to usurp this static stability, and such scenario is even less likely by warming alone considering the probable temperature range.

4.3. Thermocline depth

As mentioned earlier, the mass-exchange rate (eq. 26) may due both to the eddies and MOC, but regardless how the two may be partitioned, it represents a conversion of kinetic to potential energy in the warm water mass, thus requiring wind-work at its surface for the steady-state balance. While the importance of the wind forcing is well recognized (Huang, 1999; Wunsch, 2002), not sufficiently stressed however is the degree of freedom associated with the potential barrier itself (namely the thermocline depth), which can accommodate varying wind-work to facilitate the same mass exchange as required by the internal energy balance.

Formally, the mechanical energy balance of the warm water-mass is of the form

$$M_o \bar{h} \Delta b \approx \iint \overline{\vec{\tau} \cdot \vec{u}} \, \mathrm{d}A, \tag{32}$$

where $\bar{h}$ is the area-mean thermocline depth, Δb, the buoyancy difference across the thermocline, $\overline{\vec{\tau} \cdot \vec{u}}$, the work done by the wind stress $\vec{\tau}$ and the integration is over the warm-water surface. With M_o and Δb known from earlier derivation, the thermocline depth thus is linked to the wind-work at the warm surface, which defines in essence the Monin-Obukov scale (see Turner, 1979). For a crude estimate, one may use the mass exchange rate and buoyancy difference determined above and an average work of 10^{-3} W m^{-2} done by the wind on the warm surface that extends to 40 latitudinal degrees (Wunsch, 1998, his section 4), which would yield a mean thermocline depth of 500 m. Since we have neglected dissipation in eq. (32), this estimate represents an upper bound. One recognizes as well that the observed thermocline varies greatly in depth, ranging from less than 100 m in the tropics to a maximum of about 1000 m just before it outcrops, the Monin-Obukov scale nonetheless gives the correct order-of-magnitude estimate of its mean depth.

5. Summary and discussion

As a logical progression of a deductive climate theory (Ou01; Ou06), we have considered three climate features pertaining to the humidity profile, the atmospheric water transport, and the ocean stratification—taking as given the thermal properties previously determined. Being among the defining characteristics of the earth's climate, they all have been examined to some degree in the literature, but the main difference here lies in their addressing within the closure of a coupled system, which has led to new implications—particularly as regards climate-change studies. We shall summarize below the main findings and discuss some these implications.

5.1. Humidity profile

It is deduced that MEP leads to maximization of the net radiative cooling, which propels the ambient temperature and specific humidity to their updraft values, with the departure being constrained by the entropy and energy balances. Because of the low efficiency of the atmospheric heat engine, the CAPE is small or the thermal field is homogenized to that of the deep updrafts. This deduction may explain why in the free troposphere the lapse rate is moist-adiabatic—even though deep updrafts occupy only a small fraction of the global surface, and why the convective flux should be dominated by the latent heat. Since the radiative cooling rate does not vary strongly with height, it is deduced that the ambient vapour pressure should trend as the saturation curve, giving rise to a relative humidity that is bi-modal in the vertical—both are pronounced features in observations.

The deduction of the moisture profile has bridged a significant gap in the closure of Ou01. Since the radiative cooling as well as its effective cooling temperature is strongly modified by cloud covers (Stephens and Webster, 1979; Held et al., 1993), which in turn are internal variables, one is deterred from applying MEP to the source term (eq. 7) in constraining the global-mean fields. Rather, on account of the conversion of this irreversible entropy to the available potential energy and—hence—dissipation, Ou01 determines the global-mean state by maximizing the surface dissipation. One recognizes however that much of the irreversible entropy production may be due to moisture processes that do not generate mechanical work, and some of this work moreover is dissipated outside the PBL through turbulent cascade or frictional drag on hydrometeors, Ou01's closure thus may be justified only if all these processes do not vary as strongly with the surface temperature as the surface dissipation, which must be regarded as an assumption.

The closure of the moist convection is a topic of much discussion in the literature, but remains unresolved since most schemes hinge on unknown empirical parameters (Craig, 1996; Emanuel and Bister, 1996; Renno and Ingersoll, 1996). The present formulation however offers a plausible physical closure: the key step being the linkage of the cumulus mass flux to the high-cloud cover, which is thus constrained by global-mean energy balance (Ou01). Such closure is supported by Ou01's deduction of the observed surface temperature even with interactive cloud covers—the latter evidently a necessary element in any physical explanation of the earth's surface temperature.

Since the ambient temperature and humidity are referenced to their updraft values with the departure constrained by global balances, the tacit assumption is that the vertical advection dominates the heat and moisture balances in the deep updraft while

the horizontal mixing dominates these balances in the ambient air. This differential mixing stems from the vast disparity in the vertical air motion (more than two orders-of-magnitude) between the two regions, which in turn arises from the smallness of the updraft area. As such, the model has downplayed the importance of subsidence, which may not balance the radiative cooling and has little effect on the observed thermal and moisture profiles. It is suggested therefore that in numerical simulation of these profiles, higher premium be placed on resolving synoptic eddies that dominate the horizontal mixing than capturing the weak subsiding motion.

In terms of humidity change in a warmer climate, say, caused by doubling of the atmospheric CO_2, it is noted that since the greenhouse effect is saturated (Section 2.1), the energy balance is only slightly perturbed, so are the convective heat flux eq. (14), cumulus mass flux (Ou01) and hence the humidity deficit eq. (13)—when compared with the CC scaling. With these constraints, some inferences can be drawn. For example, since the convective heat flux is mainly in the latent form, it is proportional to the vapour flux or the global precipitation. The strength of the hydrological cycle, though slightly enhanced, thus is not sensitive to warming (Held and Soden, 2006, their fig. 2).

Moreover, since it is the humidity deficit from the saturation that is being constrained by energy balances eq. (13), one expects the high relative humidity near the surface to persist with warming. To see this more clearly, we express the humidity deficit as $q' = q_s(1 - r)$ with q_s being the saturation specific humidity and r the relative humidity, so the perturbation form of eq. (13) yields

$$\delta r = (1 - r)\left[\frac{\delta q_s}{q_s} - \frac{\delta F_c}{F_c} + \frac{\delta M_c}{M_c}\right] \tag{33}$$

$$\approx (1 - r)\frac{\delta q_s}{q_s}, \tag{34}$$

given the above constrains. We see therefore that where the relative humidity is high, it would be little changed (for a relative humidity of 0.8, for example, it increases by about 0.014 with 1 K warming). In fact, since the convective heat flux slightly increases (Held and Soden, 2006) and the convective mass flux slightly decreases (see footnote 2 and fig. 5 of Ou01), the neglected terms in (34) would partly counter the CC scaling to further stiffen the (high) relative humidity near the surface. On the other hand, since the change in the relative humidity can be substantial where the air is dry, one may not assume fixed relative humidity profile (Manabe and Wetherald, 1967), which in any event is not supported by observations (Sun and Oort, 1995). Our logic also differs from Held and Soden (2006) who assumed a fixed relative humidity to argue for a strongly decreasing mass flux to counter the CC scaling eq. (33), whereas in our formulation it is the relatively unchanging mass flux due to energy balance that maintains the high relative humidity near the surface. When assessing the convective mass flux from climate models, one should be mindful that this flux can be properly captured only if the models have resolved the cumulus convection and that there remains considerable variance—even the sign of the change—among model predictions (see Pierrehumbert, 1999) and observed trends (Mitas and Clement, 2005).

5.2. Atmospheric water transport

Given the deduction of similar humidity profile in the ambient as in the deep updraft and the dominance of eddy transport at mid-latitudes, we determine the partition of the sensible and latent heat transports, whose dependence on the surface temperature agrees with observations. As such, the atmospheric water transport is linked to the thermal field and hence governed by the energy balance as well. It increases with both the heat transport and the surface temperature, thus has a maximum slightly equatorward of the maximum heat transport, as indeed observed.

Although extremely crude, the model nonetheless underscores the internal control of the atmospheric water transport, which thus may not be independently varied to probe the response of the system. In fact, eqs (23) and (25) together may provide physically based parametrization of the atmospheric water transport in models that do not explicitly resolve the hydrological cycle. It is recognized that variation in the freshwater transport in some climate-change studies is attributed to the anomalous ice melt, but then it must be subjected to ice-mass balance (Rahmstorf, 1995), a constraint not sufficiently acknowledged.

One can see from (25) that the atmospheric water transport responds more strongly to warming than the strength of the hydrological cycle discussed earlier (Section 5.1). This is because the inverse Bowen ratio is only about $^1/_2$ in the presently climate (see Fig. 4), so there is room for substantial increase in the transport of the latent heat (hence water)—at the expense of that of the sensible heat as the total heat transport, being constrained by energy balance, is only slightly perturbed. These opposite trends are quite pronounced in climate models (Held and Soden, 2006), which thus can be explained. Since divergence in the horizontal water transport determines the E-P, a warmer climate thus would be characterized by an accentuated zonal-mean E-P pattern (Held and Soden, 2006)—even though the global precipitation rate remains largely unchanged. Moreover, with the local evaporation constrained by the surface energy balance, so is the local precipitation—independent of the microphysical processes that facilitate the precipitation. To reproduce the observed precipitation pattern from climate models, it is thus more important to simulate accurately the humidity profile and eddy transport processes than to incorporate detailed cloud physics.

5.3. Ocean stratification

With the atmospheric water transport derived, the mass and salt balances of the ocean then specify the salinity contrast and density ratio across the thermocline. For the present climate, the predicted density ratio is about 3, which agrees with the observed

value and moreover underscores the considerable static stability of the thermocline. Varying the wind-work would alter the thermocline depth in accordance with the Monin-Obukov scaling, but leave the thermohaline transport unchanged as demanded by the internal energy balance.

Recent climate-change studies have highlighted variability of the thermohaline circulation in response to various boundary conditions imposed at the ocean surface (e.g. Weaver et al., 1993), including its possible shut down when the freshwater flux is sufficiently high (Huang, 1994; Schmittner and Stocker, 1999). It should be stressed first of all that in a coupled system the ocean surface is merely an internal boundary, thus cannot be assigned extraneous conditions. Secondly, whatever the change in the thermohaline circulation, it should still satisfy the energy balance of the coupled system. Failure to examine such balance in fact calls into question some variability produced from ocean-only models. In the unlikely scenario that the density gradient between the warm and cold water-masses should reverse, a solution consistent with the energy balance is simply the switching of the mixing regimes, so the warm water (being denser now) fills the bulk of the ocean, while the cold water is underlain by a thermocline; the MOC is reversed, but the surface temperature and ocean heat transport remain unchanged.

In a slightly warmed climate, the increase in the atmospheric water transport would enhance the salinity contrast and reduce the density stratification across the thermocline. But since the turbulent wind may be weaker according to Ou01 (his fig. 5), the change in the thermocline depth via (32) is less certain.

Acknowledgments

I want to thank my colleagues at Lamont-Doherty Earth Observatory for spirited discussions on climate problems through the years. I want to thank Dr. Jay Fein of NSF for supporting the work through grant ATM-03–34731. Lamont-Doherty Earth Observatory contribution number: 7032.

Referrences

Bryan, F. 1986. High-latitude salinity effects and interhemispheric thermohaline circulation. *Nature* **323**, 301–304.

Craig, G. C. 1996. Dimensional analysis of a convecting atmosphere in equilibrium with external forcing. *Q. J. R. Meteorol. Soc.* **122**, 1963–1967.

Dessler, A. E. and Sherwood, S. C. 2000. Simulations of tropical upper tropospheric humidity. *J. Geophys. Res.* **105,** 20155–20163.

Emanuel, K. A. 1994. *Atmospheric Convection*. Oxford University Press, York, 580 pp.

Emanuel, K. A. and Bister, M. 1996. Moist convective velocity and buoyancy scales. *J. Atmos. Sci.* **53** (22), 3276–3285.

Emanuel, K. A., Neelin, J. D. and Bretherton, C. S. 1994. On large-scale circulations in convecting atmospheres. *Q. J. R. Meteorol. Soc.* **120**, 1111–1143.

Folkins, I., Kelly, K. K. and Weinstock, E. M. 2002. A simple explanation for the increase in relative humidity between 11 and 14 km in the tropics. *J. Geophys. Res.* **107** (D23), 4736, doi:10.1029/2002JD002185

Hartmann, D. L. and Michelsen, M. L. 1993. Large-scale effects on the regulation of tropical sea surface temperature. *J. Climate* **6**, 2049–2062.

Held, I. M., Hemler, R. S. and Ramaswamy, V. 1993. Radiative-convective equilibrium with explicit two-dimensional moist convection. *J. Atmos. Sci.* **50**, 3909–3927.

Held, I. M. and Soden, B. J. 2000. Water vapor feedback and global warming. *Annu. Rev. Energy Environ.* **25**, 441–475.

Held, I. M. and Soden, B. J. 2006. Robust responses of the hydrological cycle to global warming. *J. Climate* **19**, 5686–5699.

Huang, R. X. 1994. Thermohaline circulation: energetics and variability in a single-hemisphere basin model. *J. Geophys. Res.* **99,** 12,471–12,485.

Huang, R. X. 1999. Mixing and energetics of the oceanic thermohaline circulation. *J. Phys. Oceanogr.* **29**, 727–746.

Kleidon, A., Fraedrich, K., Kunz, T. and Lunkeit, F. 2003. The atmospheric circulation and states of maximum entropy production. *Geophys. Res. Lett.* **30**(23), 2223, doi:10.1029/2003GL018363.

Kleidon, A., and Lorenz, R. D. 2005. *Non-equilibrium Thermodynamics and the Production of Entropy: Life, Earth, and Beyond*. Springer, Heidelberg, 260 pp.

Knutson, T. R. and Manabe, S. 1995. Time-mean response over the tropical Pacific to increased CO2 in a coupled ocean-atmosphere model. *J. Climate* **8**, 2181–2199.

Lorenz, E. N. 1967. *The Nature and Theory of the General Circulation of the Atmosphere*. World Meteorological Organization, Geneva, 161 pp.

Lorenz, R. D. and McKay, C. P. 2003. A simple expression for vertical convective fluxes in planetary atmospheres. *Icarus* **165**, 407–413.

Manabe, S. and Strickler, R. F. 1964. Thermal equilibrium of the atmosphere with a convective adjustment. *J. Atmos. Sci.* **21**, 361–385.

Manabe, S. and Stouffer, R. J. 1994. Multiple-century response of a coupled ocean-atmosphere model to an increase of atmospheric carbon dioxide. *J. Climate* **7**, 5–23.

Manabe, S. and Wetherald, R. T. 1967. Thermal equilibrium of the atmosphere with a given distribution of relative humidity. *J. Atmos. Sci.* **24**, 241–259.

Mitas, C. M. and Clement, A. 2005. Has the Hadley cell been strengthening in recent decades? *Geophys. Res. Lett*. **32**, L03809, doi:10.1029/2004GL021765.

Neumann, G. and Pierson, W. J. Jr. 1966. *Principles of Physical Oceanography*. Prentice-Hall, Englewood Cliffs, NJ, 545 pp.

Ou, H. W. 2001. Possible bounds on the earth's surface temperature: from the perspective of a conceptual global-mean model. *J. Climate* **14**, 2976–2988.

Ou, H. W. 2006. Thermal properties of a coupled ocean-atmosphere: a conceptual model. *Tellus* **58** (3), 404–415.

Ozawa, H., Ohmura, A., Lorenz, R. D. and Pujol, T. 2003. The second law of thermodynamics and the global climate system: a review of the maximum entropy production principle. *Rev. Geophys.* **41**, 4/10182003.

Pauluis, O. and Held, I. M. 2002. Entropy budget of an atmosphere in radiative-convective equilibrium. Part I: maximum work and frictional dissipation. *J. Atmos. Sci.* **59** (2), 125–139.

Peixoto, J. P. and Oort, A. H. 1992. *Physics of Climate*. American Institute of Physics, New York, 520 pp.

Pierrehumbert, R. T. 1995. Thermostats, radiator fins, and the local runaway greenhouse. *J. Atmos. Sci.* **52**, 1784–1806.

Pierrehumbert, R. T. 1998. Lateral mixing as a source of subtropical water vapor. *Geophys. Res. Lett.* **25** (2), 151–154.

Pierrehumbert, R. T. 1999. Subtropical water vapor as a mediator of rapid global climate change. In: *Mechanisms of Global Change at Millennial Time Scales* (eds P. U. Clark, R. S. Webb, and L. D. Keigwin). American Geophysical Union, Washington, DC, Geophysical Monograph Series 112, 394 pp.

Pierrehumbert, R. T. and Roca, R. 1998. Evidence for control of Atlantic Subtropical humidity by large scale advection. *Geophys. Res. Lett.* **25**, 4537–4540.

Rahmstorf, S. 1995. Bifurcations of the Atlantic thermohaline circulation in response to changes in the hydrological cycle. *Nature* **378**, 145–149.

Renno, N. O. 1997. Multiple equilibria in radiative-convective atmospheres. *Tellus* **49A**, 423–438.

Renno, N. O. and Ingersoll, A. P. 1996. Natural convection as a heat engine: a theory for CAPE. *J. Atmos. Sci.* **53**, 572–585.

Robe, F. R. and Emanuel, K. A. 1996. Moist convective scaling: some inferences from three-dimensional cloud ensemble simulations. *J. Atmos. Sci.* **53** (22), 3265–3275.

Schmittner, A. and Stocker, T. F. 1999. The stability of the thermohaline circulation in global warming experiments. *J. Climate* **12**, 1117–1133.

Shimokawa, S. and Ozawa, H. 2002. On the thermodynamics of the oceanic general circulation: irreversible transition to a state with higher rate of entropy production. *Q. J. R. Meteorol. Soc*. **128**, 2115–2128.

Shine, K. P. and Sinha, A. 1991. Sensitivity of the earth's climate to height-dependent changes in the water vapor mixing ratio. *Nature* **354**, 382–384.

Spencer, R. W. and Braswell, W. D. 1997. How dry is the tropical free troposphere? Implications for global warming theory. *Bull. Am. Met. Soc.* **78**, 1097–1106.

Stephens, G. L. 1990. On the relationship between water vapor over the oceans and sea surface temperature. *J. Climate.* **3**, 634–645.

Stephens, G. L. and Webster, P. J. 1979. Sensitivity of radiative forcing to variable cloud and moisture. *J. Atmos. Sci.* **26**, 1542–1556.

Stommel, H. and Csanady, G. 1980. A relation between the T-S curve and global heat and atmospheric water transports. *J. Geophys. Res.* **85**, 495–501.

Sui, C. H., Lau, K. M., Tau, W. K. and Simpson, J. 1994. The tropical water and energy cycles in a cumulus ensemble model. Part I: equilibrium climate. *J. Atmos. Sci.* **51** (5), 711–728.

Sun, D.-Z. and Lindzen, R. L. 1993. Distribution of tropical tropospheric water vapor. *J. Atmos. Sci.* **50**(12), 1643–1660.

Sun, D. and Oort, A. H. 1995. Humidity–temperature relationships in the tropical troposphere. *J. Climate* **8,** 1974–1987.

Tippins, D. and Tomczak, M. 2003. Meridional turner angles and density compensation in the upper ocean. *Ocean Dyn*. **53**, 332–342.

Trenberth, K. and Caron, J. 2001. Estimates of meridional atmosphere and ocean heat transports. *J. Climate* **14**, 3433–3443.

Turner, J. R. 1979. *Buoyancy Effects in Fluids*. Cambridge University Press, Cambridge, 368 pp.

Veronis, G. 1973. Model of the world ocean circulation: I. Wind-driven, two-layer. *J. Mar. Res.* **31**, 228–288.

Weaver, A. J., Marotzke, J., Cummins, P. F. and Sarachik, E. S. 1993. Stability and variability of the thermohaline circulation. *J. Phys. Oceanogr.* **23**, 39–60.

Webster, P. J. 1994. The role of hydrological processes in ocean-atmosphere interactions. *Rev. Geophys*. **32**, 427–476.

Wunsch, C. 1998. The work done by the wind on the oceanic general circulation. *J. Phys. Oceanogr.* **28**, 2332–2340.

Wunsch, C. 2002. What is the thermohaline circulation? *Science* **298**, 1179–1180.